Displacive Phase Transitions at Large Strains: Phase-Field Theory and Simulations

Valery I. Levitas,[1] Vladimir A. Levin,[2] Konstantin M. Zingerman,[3] and Eugene I. Freiman[4]

[1]*Iowa State University, Departments of Mechanical Engineering, Aerospace Engineering, and Material Science and Engineering, Ames, Iowa 50011, USA*

[2]*Department of Mechanics and Mathematics, Lomonosov Moscow State University, Moscow, 119899 Russian Federation*

[3]*Department of Applied Mathematics and Cybernetics, Tver State University, Tver 170100 Russian Federation*

[4]*Department of Mechanics and Mathematics, Tula State University, Tula 300600 Russian Federation*

(Received 8 December 2008; revised manuscript received 13 June 2009; published 8 July 2009)

The Landau potential for multivariant displacive phase transformations (PTs) is derived for the most general case of large rotations, elastic and transformational strains, as well as nonlinear and different elastic properties of phases. The method of repetitive superposition of large strains is extended for PTs and is utilized in the finite-element method approach for solution of corresponding coupled phase-field and mechanical problems. Problems of martensitic variants nucleation and evolution in a nanosize sample, including a sample with two nanovoids, are solved. A similar approach can be applied for twinning, dislocations, and reconstructive PTs.

DOI: 10.1103/PhysRevLett.103.025702 PACS numbers: 64.70.K−, 64.60.−i, 81.30.Kf

Ginzburg-Landau (GL) or phase-field equations are broadly applied for the analysis and simulation of a wide class of stress-induced martensitic and reconstructive PTs [1–3]. Recently [3], we advanced this theory by developing a more sophisticated Landau potential that (in contrast to previous approaches) generates a stress-strain curve that is conceptually consistent with known experimental data for shape-memory alloys, steel, and ceramics. In particular, constant (stress- and temperature-independent) transformation strain tensor, nonzero elastic moduli at the PT point, and weakly temperature-dependent (in particular, constant) stress hysteresis observed experimentally can be reproduced. The main limitation of this and other theories is related to small strain and rotation (i.e., <0.1) approximation. At the same time, while the crystallographic theory of martensitic PTs completely neglects elastic strains, it takes into account large strains and rotations, which appear to be important for determination of interface orientation [4]. Finite rotation may be caused by specific loading even at small strains. The volumetric transformation strain for the PT in plutonium, silicon, and germanium is 0.2; and for the PT graphite-diamond and rhombohedral-cubic and hexagonal-wurtzitic PTs in *BN*, it is 0.54 [5,6]. For all of the above PTs, transformation strain is highly anisotropic—i.e., it contains a large deviatoric (shear) component. The transformation shear is 0.2 for PTs in steels and some shape-memory alloys and is 0.71 for twinning in bcc and fcc lattices [4–6]. Large elastic strains can be caused by high pressure. Also, in nanoscale defect-free volumes and nanofilms, large elastic strains can be caused by local stress concentrators and lattice misfit. Thus, fully geometrically and physically nonlinear phase-field theory is required, especially for nanotechnology and high-pressure applications.

For the Landau potential in terms of total strain [2] (rather than transformation strain), extension for finite deformations does not significantly complicate the theory at first glance. However, even at small strain, potentials in terms of total strain cannot describe the above-mentioned important features of stress-induced martensitic PTs [3]. The only formulation that generalizes theory [3] for large strains is given in our paper [6]. However, it was limited to neglect of elastic strains. That formulation also did not include change in elastic properties of phases, which is extremely important, for example, for PTs in BN and graphite. No large-strain simulations based on GL equations are known.

In this Letter, the Landau potential for multivariant displacive PTs is derived for the most general case of large rotations, elastic and transformational strains, and for nonlinear and different elastic properties of phases. The coupled system of time-dependent GL equations for all order parameters, characterizing transformation strain for each martensitic variant, and continuum mechanical equations is formulated. The method of repetitive superposition of large strains, developed for viscoelastic materials [7], is extended here for materials with PTs. Based on this method, the finite element method (FEM) approach, algorithm, and code for solution of the above system of equations are developed. Problems of nucleation and evolution of martensitic variants in a nanosize sample, including a sample with two nanoholes, are solved and analyzed. Note that, due to multiple nonlinearities, the traditional spectral method [1] cannot be used. It also would have problems applying stress-free conditions at variable hole surfaces. A similar potential and approach can be applied for twinning, dislocations, reconstructive PTs, and fracture.

We designate contractions of tensors $\boldsymbol{A} = \{A_{ij}\}$ and $\boldsymbol{B} = \{B_{ji}\}$ over one and two indices as $\boldsymbol{A} \cdot \boldsymbol{B} = \{A_{ij}B_{jk}\}$ and $\boldsymbol{A}{:}\boldsymbol{B} = A_{ij}B_{ji}$. The transpose of $\boldsymbol{A}$ is $\boldsymbol{A}^T$, and $\boldsymbol{I}$ is the unit tensor.

Model.—Multiplicative decomposition of the total deformation gradient,

$$\boldsymbol{F} = \partial \boldsymbol{r}/\partial \boldsymbol{r}_0 = \boldsymbol{F}_e \cdot \boldsymbol{F}_t, \tag{1}$$

into elastic and transformational parts will be used [6,8]. Here, $\boldsymbol{r} = \boldsymbol{r}(\boldsymbol{r}_0, t)$ is the location of a material point at time t, and $\boldsymbol{r}(\boldsymbol{r}_0, 0) = \boldsymbol{r}_0$. The transformation deformation gradient (or Bain strain) $\boldsymbol{F}_{ti}$ transforms the stress-free crystal lattice of an austenite (A) into a stress-free lattice of martensitic variant M_i, $i = 1, 2, \ldots, n$, as in the crystallographic theory [4]. Deviations of $\boldsymbol{F}$ from $\boldsymbol{F}_t$ cause elastic lattice strains $\boldsymbol{F}_e$. The decomposition (1) is unique because lattice rotation is included in $\boldsymbol{F}_e$. For small strains $\boldsymbol{\varepsilon} \ll \boldsymbol{I}$ and rotations, $\boldsymbol{F} = \boldsymbol{I} + \boldsymbol{\varepsilon}$, $\boldsymbol{F}_e = \boldsymbol{I} + \boldsymbol{\varepsilon}_e$, and $\boldsymbol{F}_t = \boldsymbol{I} + \boldsymbol{\varepsilon}_t$, and Eq. (1) reduces to additive decomposition $\boldsymbol{\varepsilon} = \boldsymbol{\varepsilon}_e + \boldsymbol{\varepsilon}_t$. The order parameter η_i for each M_i varies from 0 (corresponding to A and $\boldsymbol{F}_t = \boldsymbol{I}$) to 1 (corresponding to M_i). Substituting the Helmholtz free energy $\psi(\boldsymbol{F}_e, \theta, \eta_i)$ into the second law of thermodynamics, $D = \boldsymbol{P}^T{:}\dot{\boldsymbol{F}} - \dot{\psi} \geq 0$, where D is the dissipation rate and $\boldsymbol{P}$ is the nonsymmetric Piola-Kirchoff stress tensor $\boldsymbol{P}$ (force per unit area in the undeformed configuration), we obtain, at constant temperature θ,

$$\begin{gathered} \boldsymbol{P} \cdot \boldsymbol{F}_t^T = \frac{\partial \psi}{\partial \boldsymbol{F}_e}; \qquad D = X_i \dot{\eta}_i \geq 0, \\ X_i := \boldsymbol{P}^T \cdot \boldsymbol{F}_e{:}\frac{\partial \boldsymbol{F}_t}{\partial \eta_i} - \frac{\partial \psi}{\partial \eta_i}. \end{gathered} \tag{2}$$

Equation (2)1 is the elasticity rule, Eq. (2)2 is the dissipative inequality, and X_i is the driving force for PT to the ith variant. The corresponding GL equation is

$$\partial \eta_k/\partial t = \sum_{i=1}^{n} L_{ki}(X_i + 2\boldsymbol{\beta}_i{:}\boldsymbol{\nabla}\boldsymbol{\nabla}\eta_i), \tag{3}$$

where L_{ki} are the kinetic coefficients and $\boldsymbol{\beta}_i$ is the second-rank gradient-energy tensor. The explicit expression for the ψ is derived in the following form:

$$\psi = \mathcal{A}(\mathbf{E}_e, \eta_i) + \sum_{k=1}^{n} f(\eta_k) + \sum_{i=1}^{n-1}\sum_{j=i+1}^{n} F_{ij}(\eta_i, \eta_j), \tag{4}$$

with

$$\begin{gathered} \mathbf{E_e} = (\mathbf{F}_e^T \cdot \mathbf{F}_e - \mathbf{I})/2, \\ f(\eta_k) = A\eta_k^2(1-\eta_k)^2 + \Delta G^\theta(4\eta_k^3 - 3\eta_k^4), \end{gathered} \tag{5}$$

$$\begin{aligned} F_{ij}(\eta_i, \eta_j) = {} & B\eta_i\eta_j(1-\eta_i-\eta_j)[(\eta_i-\eta_j)^2 - \eta_i - \eta_j] \\ & + D\eta_i^2\eta_j^2(1-\eta_i-\eta_j) + \eta_i^2\eta_j^2(\eta_i+\eta_j) \\ & \times (\bar{A} - A) + \eta_i^2\eta_j^2(\eta_i T_i + \eta_j T_j). \end{aligned} \tag{6}$$

Here, $\mathcal{A}$ is the elastic potential, $\mathbf{E_e}$ is the Lagrangian elastic strain tensor, and ΔG^θ is the difference between the thermal parts of the free energies of M and A. The parameters A and $\bar{A}$ represent the thresholds for the $\mathsf{A} \leftrightarrow \mathsf{M}_i$ and $\mathsf{M}_j \leftrightarrow \mathsf{M}_i$ PTs. The constants B and D do not contribute to phase equilibrium and instability conditions. However, they affect the free energy far from the A and M_i minima and the minimum-energy paths between the A and M_i, which means that they control the interface energy and kinetics of PT. Also, they are used to avoid nonphysical energy minima that may appear for such a complex polynomial [3]. As an example, we consider the Murnaghan potential:

$$\begin{aligned} \mathcal{A}(\mathbf{E}_e, \eta_i) = {} & 0.5\lambda(\eta_i){E_1}^2 + \mu(\eta_i)E_2 + C_3(\eta_i){E_1}^3 \\ & + C_4(\eta_i)E_1E_2 + C_5(\eta_i)E_3, \end{aligned} \tag{7}$$

where $E_m = {\mathbf{E}_e}^m{:}\mathbf{I}$ ($m = 1, 2, 3$) are the invariants of $\mathbf{E}_e$; and λ, μ, and C_i are elastic moduli that depend upon η_i in the same way—e.g.,

$$\lambda = \lambda_0 + \sum_{k=1}^{n}(\lambda_k - \lambda_0)g(\eta_k), \qquad g(\eta_k) = 3\eta_k^2 - 2\eta_k^3, \tag{8}$$

where subscript 0 is for A and k is for M_k. Then, the parameters T_i in Eq. (6) are

$$\begin{aligned} T_i = -3[& 0.5(\lambda_i - \lambda_0){E_1}^2 + (\mu_i - \mu_0)E_2 + (C_{3,i} - C_{3,0}){E_1}^3 \\ & + (C_{4,i} - C_{4,0})E_1E_2 + (C_{5,i} - C_{5,0})E_3]. \end{aligned} \tag{9}$$

For the isotropic potential, all elastic constants with all $i \neq 0$ are equal. For general anisotropic potential $\mathcal{A}(\mathbf{E}_e, \boldsymbol{C}_k, \eta_i) = \boldsymbol{E}_e{:}\boldsymbol{C}_2(\eta_i){:}\boldsymbol{E}_e/2 + (\boldsymbol{E}_e{:}\boldsymbol{C}_3(\eta_i){:}\boldsymbol{E}_e){:}\boldsymbol{E}_e/3 + \ldots$, where tensors of elastic moduli of rank k, $\boldsymbol{C}_k$, are determined by an equation similar to Eq. (8), and one obtains

$$T_i = -3\mathcal{A}(\mathbf{E}_e, \boldsymbol{C}_{k,i} - \boldsymbol{C}_{0,i}). \tag{10}$$

The transformational part of the deformation gradient is

$$\mathbf{F}_t = \mathbf{I} + \sum_{k=1}^{n} q(\eta_k)\boldsymbol{\varepsilon}_{tk} - \sum_{i=1}^{n-1}\sum_{j=i+1}^{n} \eta_i^2\eta_j^2(\eta_i\mathbf{Z}_{ij} + \eta_j\mathbf{Z}_{ji}), \tag{11}$$

$$\begin{gathered} \mathbf{Z}_{ij} = (a-3)\boldsymbol{\varepsilon}_{tj} + 3\boldsymbol{\varepsilon}_{ti}, \qquad \boldsymbol{\varepsilon}_{tk} = \mathbf{F}_{tk} - \mathbf{I}, \\ q(\eta_k) = a\eta_k^2(1-\eta_k)^2 + (4\eta_k^3 - 3\eta_k^4), \end{gathered} \tag{12}$$

where a is the parameter. The method to derive Eqs. (4)–(12) is similar to that in [3] for small strains. We formulated the same requirements as in [3] that the Landau potential has to satisfy, and we derived Eqs. (4)–(12) that satisfy them for large strain. Thus, Eqs. (4)–(12) describe correctly the $\mathsf{A} \rightarrow \mathsf{M}_i$ and $\mathsf{M}_i \rightarrow \mathsf{M}_j$ PTs and the typical experimentally observed features of stress-strain curves, and they also incorporate all thermomechanical properties of the A and M. Equation (11) for $\boldsymbol{F}_t$ is independent of stress and temperature at M_i. The main step, which (in contrast to [3,6]) allowed us to make a proper generalization for large elastic strains and take into account different nonlinear elastic properties of phases, is related to formulation of the Landau potential in terms of Lagrangian elastic strains (rather than stresses). As a result, the only difference between Eqs. (4)–(12) from their small-strain counterparts is substitution of small elastic and transformation strains with their finite-strain counterparts. Essential geometric nonlinearities are separated from the potential and con-

tained in Eqs. (1) and (2). In the small-strain limit, Eqs. (1)–(12) are equivalent to the theory presented in [3]. Equations (1)–(12) are supplemented by the equilibrium equation in a deformed state: $\nabla \cdot \boldsymbol{\sigma} = 0$, where $\boldsymbol{\sigma} = \boldsymbol{P} \cdot \boldsymbol{F}^T / \det \boldsymbol{F}$ is the true Cauchy stress [8].

Material parameters for cubic to tetragonal PT in NiAl found in [3,6] are: $A = 0.8$ GPa, $\Delta G = -0.315$ GPa, $a = 2.98$, $\bar{A} = 5.32$ GPa, $B = 0$, $D = 0.5$ GPa, $L_{ii} = 2600$ (Pa s)$^{-1}$, $L_{ij} = 0$ for $i \neq j$, $\beta = 2.588 \cdot 10^{-10}$ N [the isotropic version of GL Eqs. (3) was used]. A plane strain $2 - D$ problem with two M_i is considered with the components of $\boldsymbol{F}_t$ (1.215; 0.922; 0.922) and (0.922; 1.215; 0.922) [3,6]. Elastic constants in the potential Eqs. (7), $\lambda_0 = 144$ GPa, $\mu_0 = 74$ GPa, $\lambda_1 = \lambda_2 = 379$ GPa, $\mu_1 = \mu_2 = 134$ GPa, were calculated as the orientational average of anisotropic moduli taken from [3]; $C_i = 0$. The width of the $\mathsf{M}_i - \mathsf{M}_j$ interface for the stress-free case is $\Delta \sim \sqrt{\beta/A}$, and for given parameters $\Delta \simeq 1$ nm [3]. Characteristic time is $T \sim 1/(AL) \simeq 0.5$ ps and stress for $\mathsf{A} - \mathsf{M}$ PT under hydrostatic tension is estimated (with elastic strain neglected) as $\sigma = A/a/(\det \boldsymbol{F}_t - 1) = 8.1$ GPa [6]. All size, time, and stress parameters will be presented in terms of $\Delta = 1$ nm, $T = 0.5$ ps, and $\sigma_t = 10$ GPa.

The finite-element method is employed in this work. Because of multiple nonlinearities [the nonlinear elasticity law and the η_i dependence of ψ, the change in geometry, finite strains and rotations, and nonlinear decomposition (1)], the traditional spectral method [1] cannot be used. Because the energy has multiple minima, multiple stationary solutions are possible, and the solution strongly varies on the scale of Δ and may oscillate in space, special care must be taken with regard to numerical solution accuracy. Traditionally, large-strain equations have been linearized in the form of superposition of the small strains on the finite strain. Here, we extended the methods of repetitive superposition of large strains, developed in [7] for viscoelastic materials, to materials with PTs.

We study nucleation and evolution of multivariant martensitic microstructure and its growth up to stationary state. For all problems, lack of complete transformation in the entire sample is related to the presence of a plane-strain constraint. We consider a square sample of size l under biaxial loading with Cauchy stress components p_1 and p_2 at the deformed sample surface. At all boundaries, $\boldsymbol{n} \cdot \nabla \eta_k = 0$, which corresponds to the same surface energies of A and M_j, where $\boldsymbol{n}$ is the normal to the deformed boundary.

Examples of solutions.—1. Solutions to the problem with sample size $l = 27$ under stresses $p_2 = -p_1 = 0.7$ are presented in Fig. 1. Initial conditions are stochastic η_1 and η_2 homogeneously distributed in the range [0, 0.1]. Distribution a is for a geometrically linear formulation [3] in which we still add calculated displacements to the initial geometry. Figure 1(b) is for the large-strain formulation. Comparisons of the evolution of vertical stress σ_2, out-of-plane stress σ_3, and η_2 at the point shown in Fig. 1(a) for

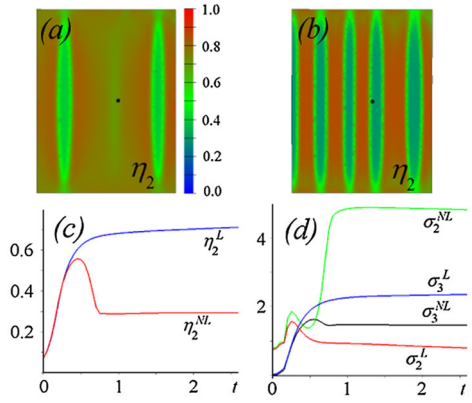

FIG. 1 (color online). (a) and (b) Stationary solutions for η_2 for the problem with sample size $l = 27$ under stresses $p_2 = -p_1 = 0.7$. The color legend is the same for all figures. Initial conditions are stochastic η_1 and η_2 homogeneously distributed in 0, 0.1. Distribution (a) is for a geometrically linear problem, and (b) is for large-strain formulation. (c) and (d) Comparison of evolution of vertical stress σ_2, out-of-plane stress σ_3, and η_2 at the point shown in Fig. 1a for geometrically linear (L) and nonlinear (NL) formulations.

geometrically linear and large-strain formulations are given in Figs. 1(c) and 1(d). In the stationary state, solutions for η_2 represent alternating bands of incomplete martensite; $\eta_1 = 0$. Microstructure based on the large-strain formulation differs qualitatively from the geometrically linear one. Specifically, it contains a larger number of bands with smaller spacing between them. A similar difference was obtained for various other initial conditions. Stresses σ_2 differ by a factor of 4.5.

2. Stationary solutions for η_1 and η_2 for the problem with sample size $l = 40.22$ under tensile stresses $p_1 = p_2 = 1.5$ are presented in Fig. 2. Initial conditions are $\eta_1 = 0.1$ and $\eta_2 = 0$ in the central circle and $\eta_1 = 0$ and $\eta_2 = 0.1$ in the two other circles with the radius of 3.35. Geometrically linear solutions (a and b) again differ qualitatively from the large-strain formulation (c and d). While in the geometrically linear case primitive alternate-twin microstructure with quite sharp interfaces is observed, the large-strain formulation results in a much more topologically sophisticated microstructure with broader interfaces.

3. The physically important problem on martensite nucleation near two nanovoids was solved in large-strain formulation. Results of simulations for a sample with $l = 40$, two symmetric holes with $r = 4.5$ (distance between holes is 14), and tensile stress $p_1 = 1.2$ and $p_2 = 0.9$, are presented for three time instants in Fig. 3. An initial perturbation $\eta_1 = \eta_2 = 0.1$ was prescribed in circles of radius 6.67 around each hole. At the free surface of the deformed holes, $\boldsymbol{n} \cdot \boldsymbol{\sigma} = 0$. The complex evolution of both embryos includes variant-variant transformation and visible change in geometry. Nucleation of M_2 starts along the horizontal symmetry axis, while M_1 nucleation occurs along vertical lines near each hole. The maximum of η_1

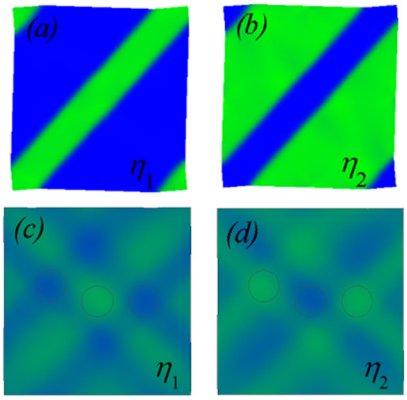

FIG. 2 (color online). Stationary solutions for η_1 and η_2 for the problem with sample size $l = 40.22$ under tensile stresses $p_1 = p_2 = 1.5$. Initial conditions are $\eta_1 = 0.1$ and $\eta_2 = 0$ in the central circle and $\eta_1 = 0$ and $\eta_2 = 0.1$ in the two other circles with the radius of 3.35. The geometrically linear solutions (a) and (b) differ qualitatively from the large-strain solutions (c) and (d).

almost reaches 1 near the hole, and η_2 reaches its maximum in the center of the sample. In the major part of a sample, M_1 dominates with $\eta_1 \simeq 0.5$.

To summarize, we derived the Landau potential for multivariant displacive PTs for the most general case of large rotations, elastic and transformational strains, and for nonlinear, anisotropic, and different elastic properties of phases. The method of repetitive superposition of large strains is extended for PTs and is utilized in the FEM approach and code for solution of corresponding coupled phase-field and mechanical problems. Problems of martensitic variant nucleation and evolution in a nanosize sample, including a sample with two nanovoids, are solved. The qualitative difference between geometrically linear and large-strain solutions is demonstrated. A similar approach can be applied for twinning, dislocations, and reconstructive PTs, as well as for PT in soft matter, where strains are very large. By including inertia (e.g., as in [9]), this approach can be easily extended to dynamic problems, and particularly shock-wave problems. Our theory can be generalized for the case of surface effects and nonsymmetry breaking degrees of freedom, as in [9]. Also, in the same way, the phase-field approach to fracture can be expanded for large strains. Both the transformation strain (simulating bond breaking) and elastic strains near the crack tip are large. The results of numerous atomistic calculations at large strain could not be presented in a practical analytical form and used in larger-scale continuum simulations because of the lack of continuum large-strain models. Our results will bridge this gap.

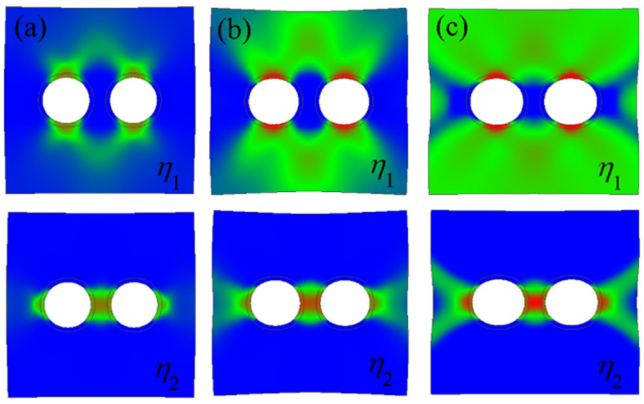

FIG. 3 (color online). Distribution of η_1 (upper row) and η_2 (lower row) (a) at time 0.42, (b) 0.63, and (c) 1.71 (a stationary solution) in a sample with $l = 40$ and two symmetric holes with $r = 4.5$ (the distance between holes is 14), and under tensile stresses $p_1 = 1.2$ and $p_2 = 0.9$.

V. I. L. acknowledges support of ARO, DTRA, NSF, and LANL, as well as discussions with D. Preston. V. A. L. acknowledges support of the NVIDIA Corporation and RFBR.

[1] Y. M. Jin, A. Artemev, and A. G. Khachaturyan, Acta Mater. **49**, 2309 (2001); L. Q. Chen, Annu. Rev. Mater. Res. **32**, 113 (2002); T. Lookman, A. Saxena, and R. C. Albers, Phys. Rev. Lett. **100**, 145504 (2008); C. J. Gagne, H. Gould, and W. Klein *et al.*, Phys. Rev. Lett. **95**, 095701 (2005); V. I. Levitas, A. V. Idesman, and D. L. Preston, Phys. Rev. Lett. **93**, 105701 (2004); V. I. Levitas and D.-W. Lee, Phys. Rev. Lett. **99**, 245701 (2007).

[2] G. R. Barsch and J. A. Krumhansl, Phys. Rev. Lett. **53**, 1069 (1984); A. E. Jacobs, S. H. Curnoe, and R. C. Desai, Phys. Rev. B **68**, 224104 (2003); S. Vedantam and R. Abeyaratne, Int. J. Non-Linear Mech. **40**, 177 (2005).

[3] V. I. Levitas and D. L. Preston, Phys. Rev. B **66**, 134206 (2002); V. I. Levitas and D. L. Preston, Phys. Rev. B **66**, 134207 (2002); V. I. Levitas, D. L. Preston, and D-W. Lee, Phys. Rev. B **68**, 134201 (2003).

[4] C. M. Wayman, *Introduction to the Crystallography of Martensitic Transformation* (Macmillan, New York, 1964); K. Bhattacharya, *Microstructure of Martensite* (Oxford University Press, Oxford, 2003).

[5] V. I. Levitas, in *High Pressure Surface Science and Engineering*, edited by Y. Gogotsi and V. Domnich (Inst. Physics, Bristol, 2004), pp. 159–292.

[6] V. I. Levitas and D. L. Preston, Phys. Lett. A **343**, 32 (2005).

[7] V. A. Levin, Int. J. Solids Struct. **35**, 2585 (1998); V. A. Levin and K. M. Zingerman, J. Appl. Mech. Trans ASME **65**, 431 (1998); V. A. Levin, *Multiple Superposition of Large Deformation in Elastic and Viscoelastic Bodies* (Moscow, Nauka, 1999).

[8] V. I. Levitas, Int. J. Solids Struct. **35**, 889 (1998); *Large Deformation of Materials with Complex Rheological Properties at Normal and High Pressure* (Nova Science Publishers, New York, 1996).

[9] A. C. Reid and R. J. Gooding, Phys. Rev. B **50**, 3588 (1994); R. J. Gooding *et al.*, Phys. Rev. B **43**, 13626 (1991).